International Journal of Fatigue 83 (2016) 100–108

Contents lists available at ScienceDirect

International Journal of Fatigue

journal homepage: www.elsevier.com/locate/ijfatigue

Effects of microstructural heterogeneity on very high cycle fatigue properties of 7050-T7451 aluminum alloy friction stir butt welds

Caiyan Deng, Hong Wang, Baoming Gong *, Xiang Li, Zhenyu Lei

Department of Materials Science and Engineering, Tianjin University, Tianjin 300072, China
Tianjin Key Laboratory of Advanced Joining Technology, Tianjin 300072, China

ARTICLE INFO

Article history:
Received 6 July 2015
Received in revised form 6 September 2015
Accepted 1 October 2015
Available online 22 October 2015

Keywords:
Friction stir welding
Aluminum alloy
Welded joint
Fatigue
Electron backscatter diffraction

ABSTRACT

In this study, the very high cycle fatigue (VHCF) properties of 7050-T7451 aluminum alloy and its friction stir welding (FSW) butt welds have been investigated. The results show that the failure of FSW joints still occurs at 7.0×10^8 cycles. The fatigue properties of the FSW joints are superior to those of the base material, especially in the super long life regime. Most fatigue cracks initiate at the thermo-mechanically affected zone and heat affected zone on the advancing side of the FSW joints, and the susceptibility of these zones to fatigue is attributed to the metallurgical heterogeneity.

© 2015 Elsevier Ltd. All rights reserved.

1. Introduction

Friction stir welding (FSW) is a typical solid-state joining technology that was invented by The Welding Institute (TWI) in 1991 [1]. FSW uses a rotating and traversing nonconsumable tool to generate frictional heat that causes mechanical deformation at the joint. The technology easily provides defect-free welds in materials with poor fusion-weldability. For instance, conventional fusion welding methods for aluminum alloys often produce some porosity in the weld metal [2,3], which deteriorates the mechanical properties, especially the fatigue properties. Therefore, FSW is widely used for the 2XXX- and 7XXX-series aluminum alloys that are known as difficult-to-weld metals [4]. Extensive studies on FSW of aluminum alloys have been performed by many researchers [5–7]. Owing to the fine recrystallization in the stir zone and the absence of the geometrical notch effect and misalignment in fusion-welded joints, it is expected that aluminum friction stir welds may have superior fracture and fatigue behavior to their fusion counterparts, and the structural reliability of FSW components can be substantially improved [8]. Lomolino et al. [9] recently suggested fatigue-life design curves for friction stir welded joints, where the fatigue strength at 2×10^6 cycles was used to identify the fatigue class as recommended by IIW [10]. However, extensive experiments have demonstrated that structural materials such as ferrous alloys, titanium alloys, and aluminum alloys exhibited no fatigue limit at 10^7 cycles or higher, and the *S–N* curve exhibited a continuous downward shape in the high cycle fatigue (HCF) regime. As a result, fatigue failure still occurred when the cycles was extended into the very high cycle fatigue (VHCF) regime [11–14]. Therefore, fatigue reliability and damage tolerance of FSW in the VHCF regime is a major concern in determining the in-service life of the FSW structural components in aerospace and aeronautical engineering.

Because the rotating FSW tool induces localized heating and plastic flow of the welded material which is followed by the rapid cooling, the heterogeneity of the microstructure in FSW is thus inevitable. Accordingly, the microstructure of the FSW joint is generally divided into three zones: the heat affected zone (HAZ), the thermo-mechanically affected zone (TMAZ), and the stir zone. The latter is characterized by an equiaxial dynamically recrystallized microstructure with strength comparable to the base material. The HAZ and TMAZ are the narrow bands between the base material and the stir zone with a relatively lower strength.

The microstructural heterogeneity gives rise to the complexity in mechanical properties of FSW joints, especially fatigue behaviors. Therefore, the fatigue properties of the FSW joint have been

Abbreviations: FSW, friction stir welding; HCF, high cycle fatigue; VHCF, very high cycle fatigue; HAZ, heat affected zone; TMAZ, thermo-mechanically affected zone; MIG, metal inert gas welding; TIG, tungsten inert gas welding; SEM, scanning electron microscopy; EBSD, electron backscatter diffraction; EDS, energy dispersive spectrometry; NDT, nondestructive testing.

* Corresponding author at: Department of Materials Science and Engineering, Tianjin University, Tianjin 300072, China.
E-mail address: gongbm@tju.edu.cn (B. Gong).

http://dx.doi.org/10.1016/j.ijfatigue.2015.10.001
0142-1123/© 2015 Elsevier Ltd. All rights reserved.

investigated by many researchers [8,15,16]. Dai et al. [15] found the highest fatigue crack propagation rate in the stir zone, which seems to violate the intuition that the fine equiaxed grains caused by recrystallization were a benefit to the fatigue performance. Ericsson and Sandström [3] reported that metal inert gas (MIG)-pulse and tungsten inert gas (TIG) welds exhibited lower static and dynamic strengths than friction stir welds. Sutton et al. [17] investigated the influence of the microstructure of FSW joints of 2024-T3 on the fracture behavior. In addition to the microstructure, the tool marks and burrs may be formed on the top surface; a lack of bonding in the weld root may appear due to the short pin. Moreover, fatigue cracks are likely to originate from such surface asperities or root flaws, resulting in inferior fatigue performance as reported in the literature [18–20].

In the study, the VHCF behavior of FSW joints of 7050-T7451 aluminum alloy is investigated and compared to that of the base material. The primary objective of the present work is to explore the relationship between the microstructural heterogeneity and the defect and VHCF properties of the FSW joints.

2. Fatigue test

The test material is a 7050-T7451 aluminum alloy rolled plate. The nominal chemical composition and mechanical properties of this material are listed in Table 1. The surface layer of the plates was ground just before the FSW process to remove the oxide layer. All of the welds were produced with the same FSW machine, and the weld axis was always parallel to the parent plate rolling direction as shown in Fig. 1. The welding parameters are listed in Table 2. No post-weld heat treatment was carried out for the joints. Fatigue test specimens with a dog-bone shape with a constant cross section in the middle gauge were extracted from the welded plates with dimensions of 250 mm × 300 mm × 12 mm (see Fig. 2). The dimensions of the specimens were determined using an analytical method to ensure that the stir zone, TMAZ and the HAZ adjacent to TMAZ resonate longitudinally at approximately 20 kHz under the same stress levels [21]. All specimens were ground and polished to a smooth finish before the fatigue tests. Fatigue testing was carried out using a piezoelectric ultrasonic fatigue machine in push–pull mode. The specimens were tested in air at room temperature with the stress ratio $R = -1$. The fatigue stress was actually derived from the displacement amplitude of the vibrating specimen. A water-cooling system was used to maintain the specimen temperature at the ambient temperature.

Scanning electron microscopy (SEM) was used for fractographical observation. The chemical compositions of the inclusions were determined by energy dispersive spectrometry (EDS). An electron backscatter diffraction (EBSD) analysis was performed using a JSM-7001F thermal field-emission scanning electron microscope with an acceleration voltage of 20 kV. Images were collected and processed by the TSL software to obtain the grain distribution and grain-boundary orientation maps of different locations on the joints.

3. Experimental results

Figure 3 shows the S–N curves of the base material and the FSW butt joints, ranging from 2 × 106 to 1 × 109 cycles. The experimental results indicate that there exists no fatigue limit in both fatigue

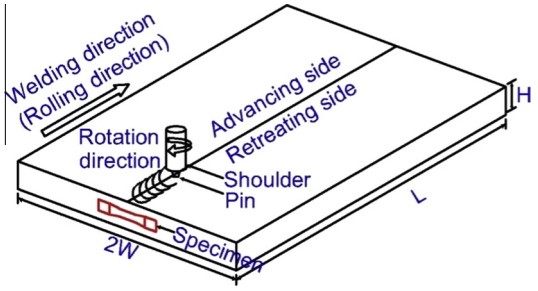

Fig. 1. Schematic of the friction stir welding (FSW) process.

Table 2
Process parameters of FSW 7050-T7451 joints.

Diameter of shoulder (mm)	Root diameter of pin (mm)	Top diameter of pin (mm)	Length of pin (mm)	Rotation speed (rpm)	Welding speed (mm/min)
25	12	6	11	300	95

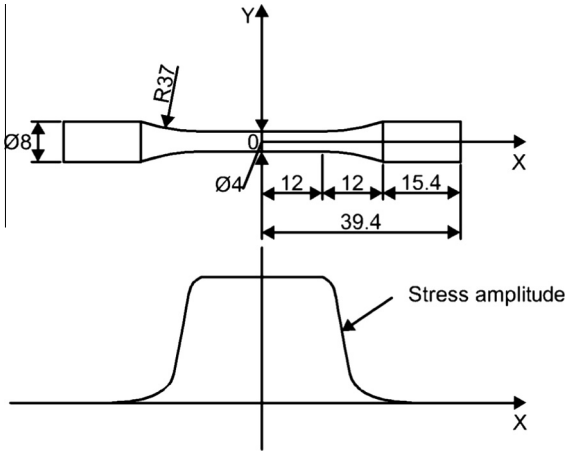

Fig. 2. The dimensions and the stress amplitude distribution of the fatigue specimen.

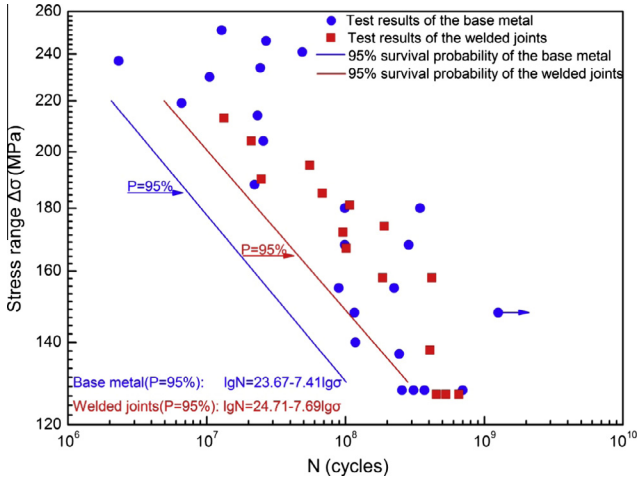

Fig. 3. The *S–N* curves for the base metal and the FSW joint.

Table 1
Chemical composition and mechanical properties of 7050-T7451 aluminum alloy.

Alloy	ρ (g cm^{-3})	σ_s (MPa)	σ_b (MPa)	E (GPa)	Zn	Mg	Cu	Fe	Si	Ti	Zr
7050	2.830	455	510	72	6.33	2.12	2.18	0.08	0.05	0.03	0.09

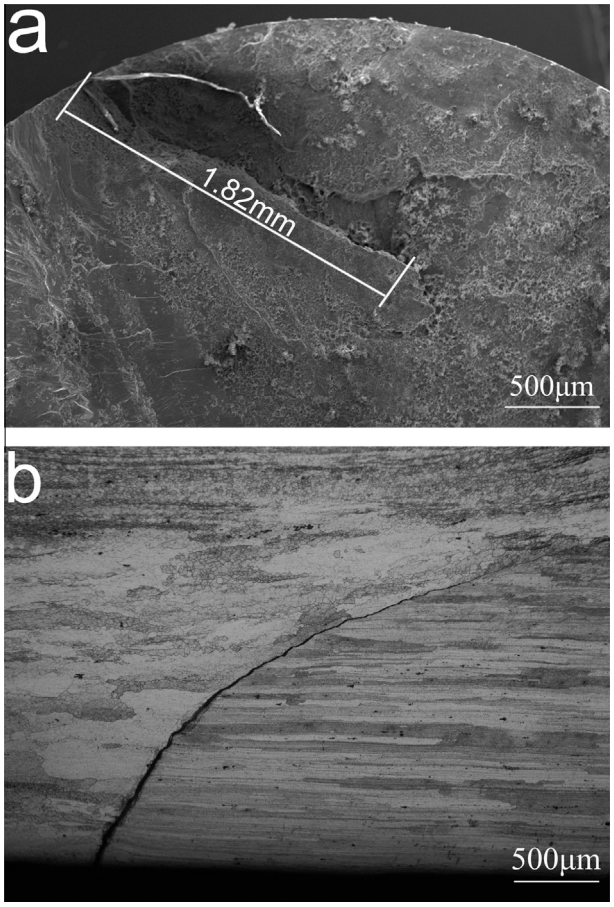

Fig. 4. Fatigue fracture surface of defective specimen (a) and incomplete penetration (b).

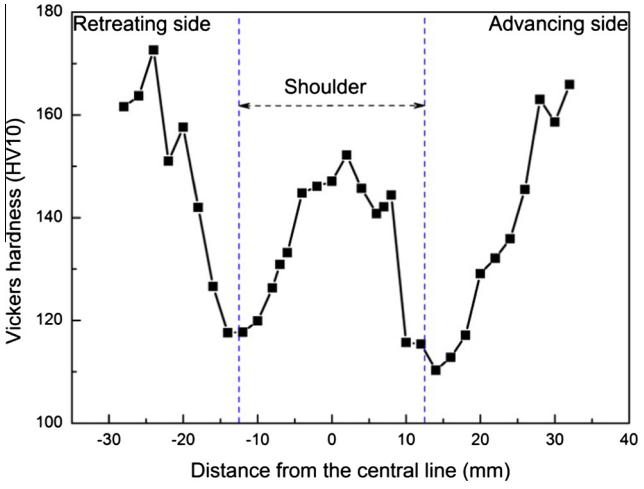

Fig. 5. Distribution of Vickers hardness (HV10) across the FSW joint.

curves. The curves still exhibit a continuously decreasing trend beyond 10^7 cycles. At 10^7 cycles, the fatigue strength of the 7050 aluminum alloy is approximately 230 MPa, consistent with the experimental results in the literature [22]. In addition, there exists a short life specimen in the tests of the welded joint. The fatigue life (5.24×10^5 cycles) of this specimen decreases dramatically, which is only 0.129% of the other specimens (4.05×10^8 cycles) at the same low stress level (138 MPa). Figure 4a shows the fatigue

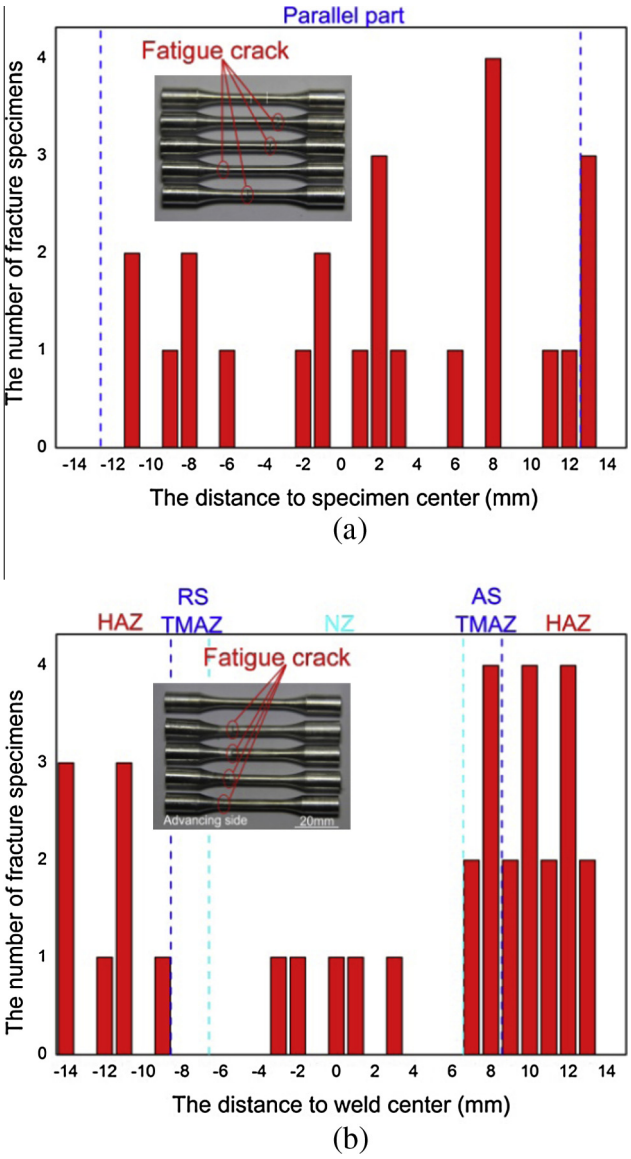

Fig. 6. Fracture positions of the specimens (a) base metal; (b) FSW joint.

specimen fracture surface with an incomplete penetration defect. Vickers hardness tests (HV10) were performed at the mid-thickness of the specimen, and the results are presented in Fig. 5.

Accordingly, it is found experimentally that the fatigue strength of the FSW joint is not only higher than that of the base material, especially in the super long life region, but the scatter band of the welded joint specimens is much narrower, which may indicate different failure mechanisms between the two. In the following discussion, we focus on the comparison of the VHCF behaviors of the FSW joint and the base material in terms of the crack initiation sites, microstructural heterogeneity, and defect effects.

4. Discussion

4.1. Preferred fatigue crack initiation site

Figure 2 illustrated schematically the distributions of the stress amplitude for a cylindrical specimen with a constant cross section in the gauge. The distribution of the stress amplitude along the experimental gauge length is almost at the same level. Statistical results for the locations of fracture of two types of specimens are

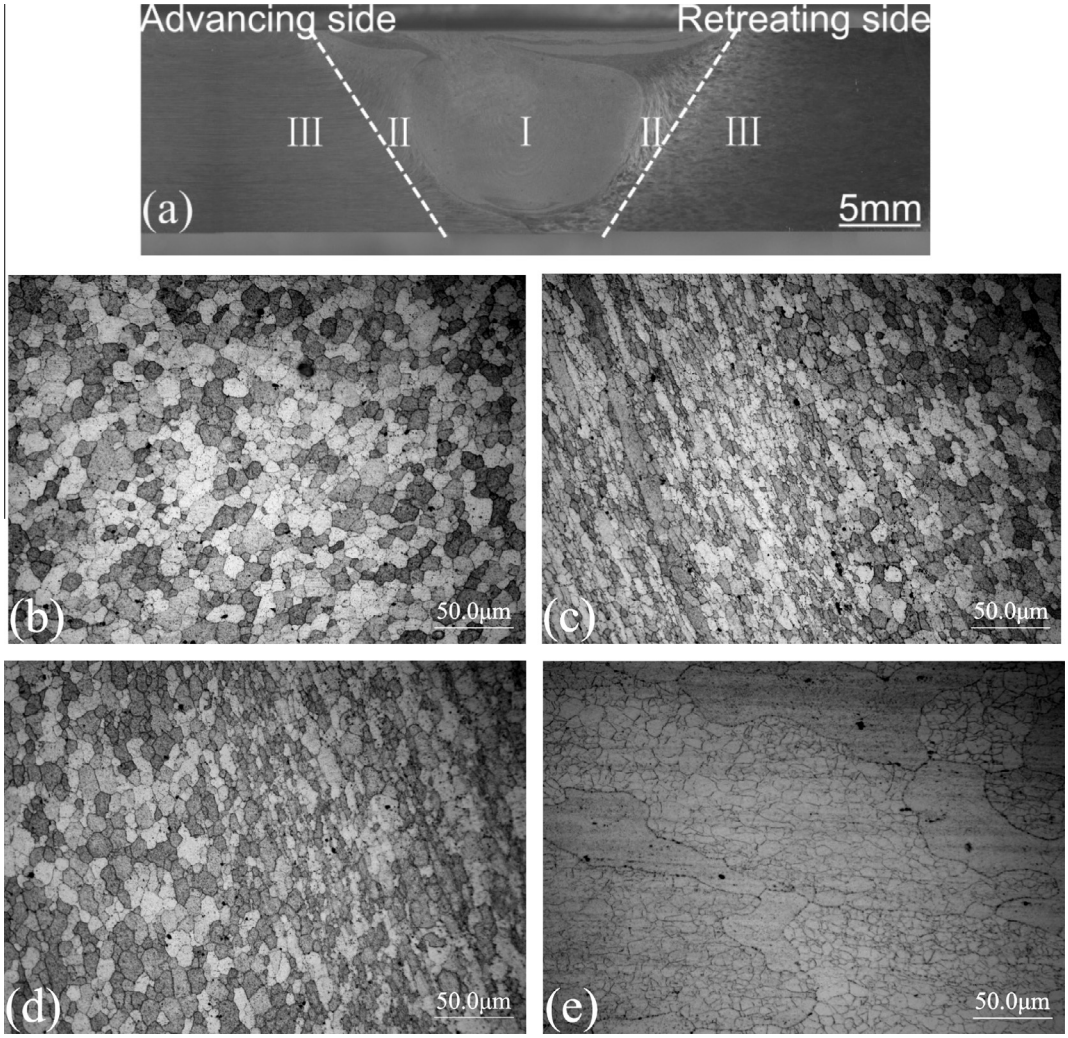

Fig. 7. Cross-section of the FSW joint for 7050-T7451 alloy (I: stir zone; II: TMAZ; III: HAZ) (a); microstructures of FSW joint at the stir zone (b); TMAZ at advancing side (c); TMAZ at retreating side (d); HAZ (e).

reported in Fig. 6. It is found that the failure positions of the base metal specimens are randomly distributed along the gauge; in contrast, only a few of specimens fracture in the stir zone of the FSW joints, and most of failure appears in the TMAZ or HAZ on the advancing side. The same phenomenon was also reported for an Al–Mg–Sc alloy in which fatigue cracks were likely to initiate on the advancing side of the stir zone [23]. Considering the mechanical and microstructural difference among the stir zone, TMAZ and HAZ, it is supposed that the phenomena are closely related to the microstructural heterogeneity and defects in FSW joint. More specifically, the preferred crack initiation site is significantly affected by the welding defects, grain orientation, load direction, etc.

4.2. Microstructural heterogeneity

Owing to the asymmetric flow of plasticized materials, these regions with distinct microstructures are shown in Fig. 7a. It can be observed in Fig. 7b that the stir zone is composed of equiaxed grains caused by dynamic recrystallization, and the homogeneous fine grains with a size of 1–10 μm are formed in this zone.

Figure 7c and d shows the grain distribution and orientation in the TMAZs of the advancing side and the retreating side, respectively. Under the effect of an insufficient thermal cycle, the grains are severely distorted and elongated at a certain angle inclined toward the original extrusion orientation of the base material. The bending of the grains in the TMAZ region suggests that the stirring action of the friction stir process causes the flat grains of the parent material to be drawn into the stir zone as shown in Fig. 7a. As a result, the grains in the TMAZ are coarsened and partly recrystallized compared to the stir zone. The difference between the microstructures on the advancing and retreating sides can be told in Fig. 7c and d. Compared with the retreating side, the distinction between the stir zone and the TMAZ can be more easily identified on the advancing side.

The grain boundary misorientation distribution of the FSW joint is investigated using the EBSD. Figure 8a–c shows the typical bimodal shape of the grains in the stir zone and TMAZ, where the peaks are located below 10° and at approximately 45°, and most of the boundaries have a high angle misorientation with greater than 15°. In contrast, the grain misorientation less than 15° at the positions of the HAZ takes up to 69.6% (see Fig. 8d). Accordingly, it is speculated that the dynamic recrystallization process accompanying plastic flow results in an increase in the density of grain boundaries. Furthermore, it is considered that a high misorientation can act as an energy barrier that hinders crack initiation and kink propagation of a crack. Jian et al. [24] analyzed the fatigue crack growth of 2124 aluminum alloy using EBSD technology and discovered

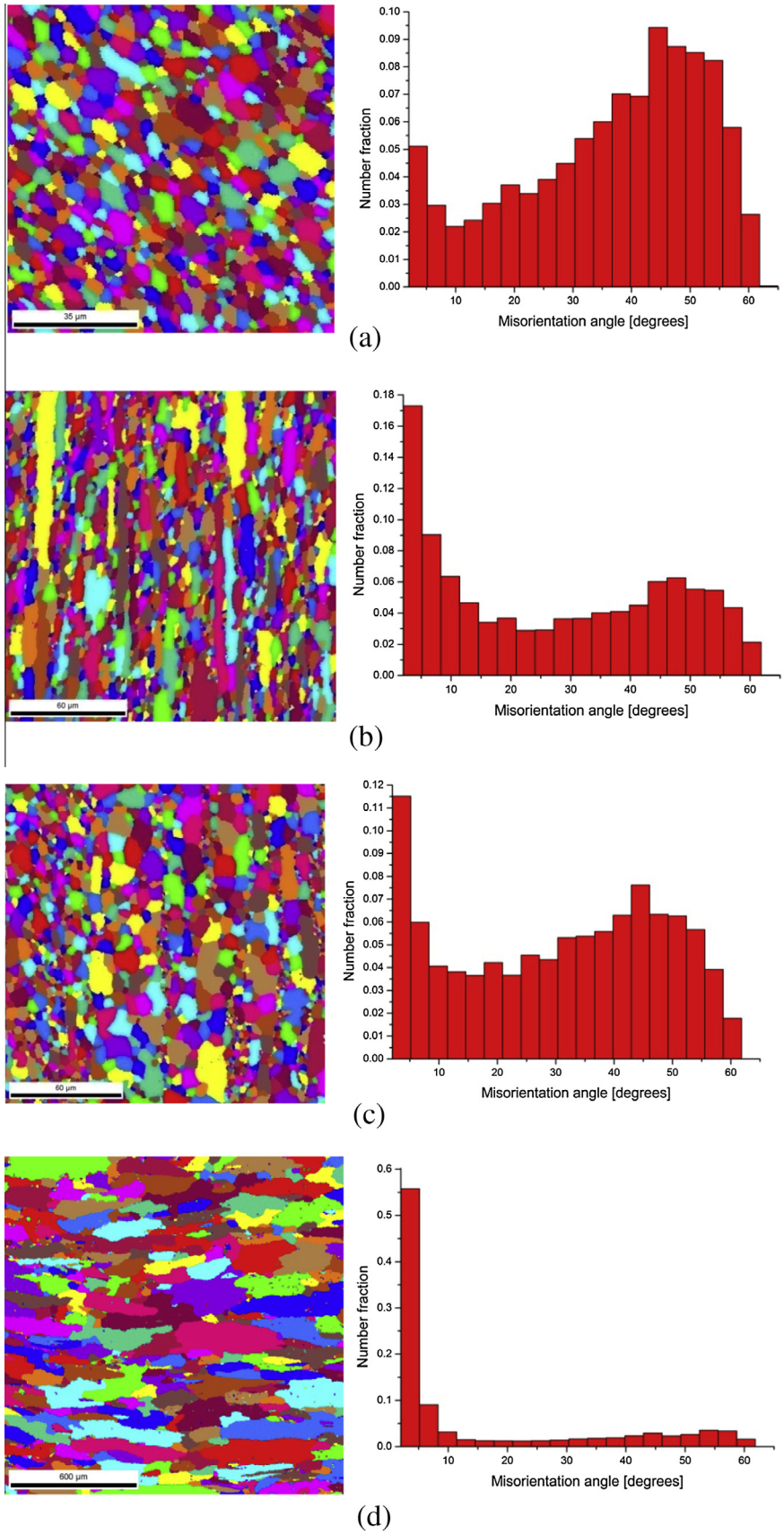

Fig. 8. Grain and misorientation angle distribution of the FSW joint for the stir zone (a); TMAZ at advancing side (b); TMAZ at retreating side (c); HAZ (d).

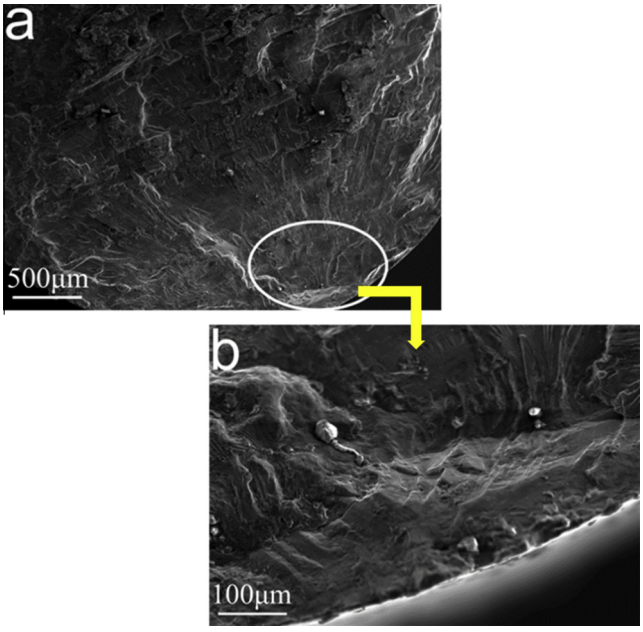

Fig. 9. Fractographic observation of the base metal: (a) low magnification; (b) high magnification at the crack source.

that the crack propagation path changes owing to the misorientation between adjoining grains. As discussed previously, the experimental results indicate that VHCF failure of the FSW specimens primarily originates on the advancing side, which was also observed by Zhou et al. [25]. The misorientation angle distribution in Fig. 8b reveals more low-angle boundaries on the advancing side. Although the grain morphology and size in the vicinity of the HAZ and the TMAZ on the retreating side are similar to those on the advancing side, the different plastic flow of the weld and the base metals on the two sides leads to different thermal cycle effects. The temperature on the retreating side is higher than that on the advancing side [26], and recrystallization proceeds more sufficiently and results in much more high-angle grain boundaries. The analysis is also consistent with the hardness profile in Fig. 5. Since the alloy is mainly strengthened by solid-solution and work hardening, the local softening of the FSW joint is usually attributed to the strengthening precipitates dissolving. It is found in Fig. 5 that a significant decrease in the hardness is observed on the advancing and retreating sides in the HAZ, equal to 65% of the parent metal hardness. Regarding to the HAZ hardness, no significant difference from the base material could be observed due to a limited influence of the welding thermal cycle. Furthermore, owing to grain-boundary migration resistance and a lack of recrystallization dynamics, the growth of grains in the HAZ is severely constrained by the initial grain size, and the strengthening precipitates may further coarsen [27]. As a result, the minimum hardness is found in the HAZ on the advancing, which tends to be a relatively weak link.

Considering the metallurgical heterogeneity during the FSW process, it is concluded that there may exist 'notch effects' on the advancing side of the FSW joint which leads to inferior crack initiation threshold in the gigacycle fatigue; the local softening is also able to characterize by the Vickers hardness profile and the misorientation distribution comprised of low-angle boundaries. It is usually assumed that the former is in favor of crack initiation, and the latter can reduce the crack propagation resistance significantly.

4.3. Fractographic observation

The crack sources in the specimens can be divided into two different types, namely, surface and internal ones. Subsurface inclusions and incomplete penetration are usually identified as the latter. It is found in Fig. 9 that the fracture surface of the base metal is relatively flat with a crack initiating at the surface. As regards the FSW joint observed in Fig. 10, the crack also originates from the surface of the specimen, even though a noticeable welding defect exists in the interior of the section.

Based on the extensive experimental observation, Hong et al. considered that there was a competition between surface crack initiation and interior crack initiation in the VHCF [28]. It is concluded that the fatigue life increases as the size of inclusion

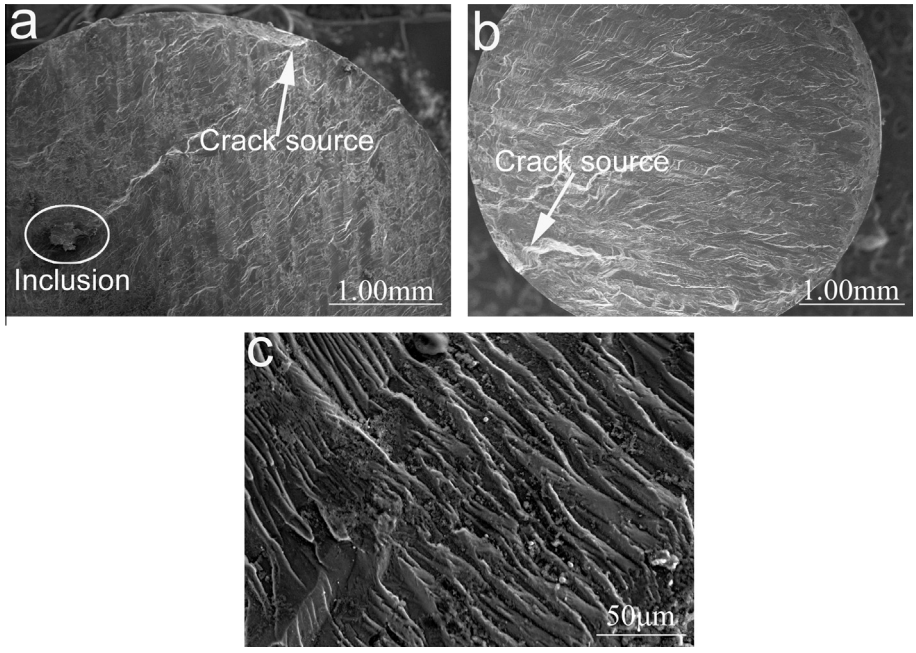

Fig. 10. Fractographic observation of the FSW welded joints.

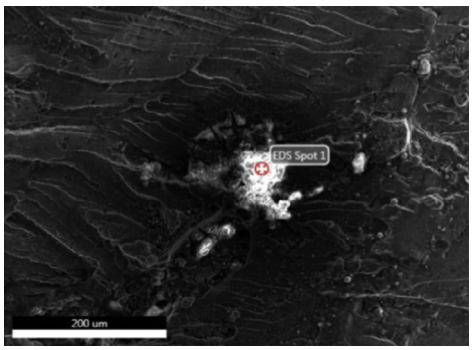

Element	Weight %	Atomic %
C K	20.54	30.87
O K	43.92	49.56
NaK	0.71	0.56
MgK	0.70	0.52
AlK	22.14	14.82
MoL	1.44	0.27
FeK	10.55	3.41

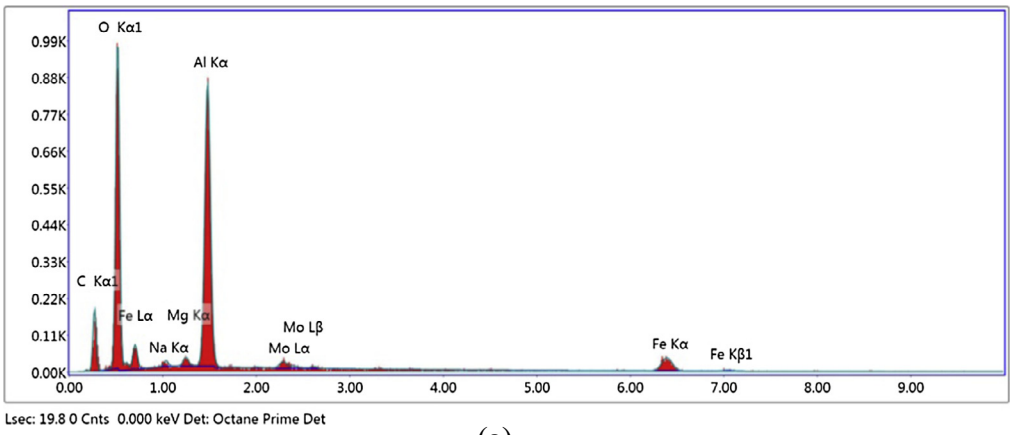

(a)

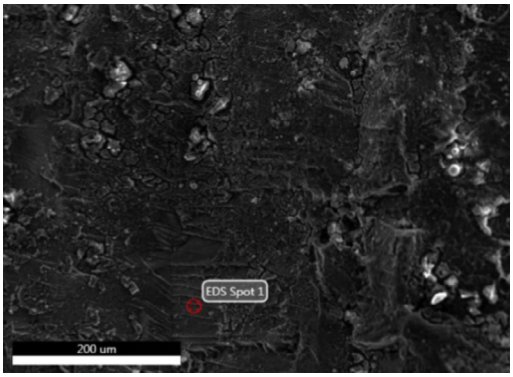

Element	Weight %	Atomic %
O K	6.02	10.08
MgK	2.53	2.79
AlK	84.96	84.46
ZnK	6.49	2.66

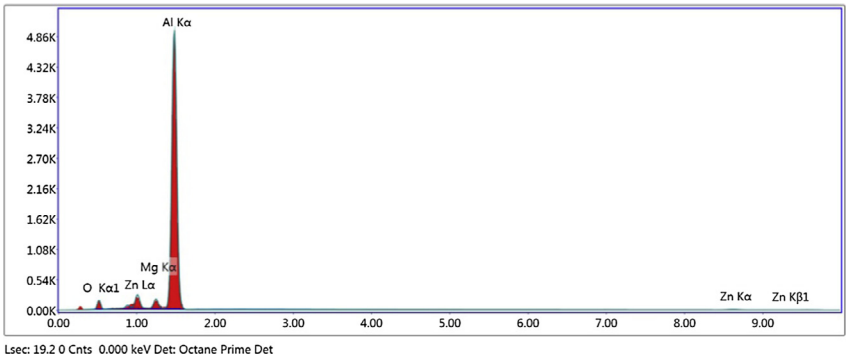

(b)

Fig. 11. EDS analysis for the inclusion (a); the FSW joint substrate (b).

decreases or the distance from the inclusion to the surface increases [29]. Therefore, considering the location of the internal inclusion, surface or sub-surface defect dominates the crack initiation for the case.

4.4. Defect effects

Although the FSW joint is exempt from the defects associated with fusion welding, there still exist some unique defects such as

Table 3
Fatigue strength of specimens (1×10^7, 1×10^8 and 1×10^9).

Status	$\Delta\sigma$ (MPa) (1×10^7)	$\Delta\sigma$ (MPa) (1×10^8)	$\Delta\sigma$ (MPa) (1×10^9)
Base metal specimen	230	169	124

burrs and flash, grooves, streaks, cavities, zigzag lines, and incomplete penetration. In the section, the effects of inclusions and incomplete penetration for gigacycle fatigue are analyzed.

4.4.1. Inclusions

Through an EDS analysis, the inclusions in Fig. 11 are identified as Al_2O_3. Owing to an inappropriate pretreatment, either the oxide layer or the non-removed dust and oil remnant on the surface of the aluminum alloy was not entirely broken and subsequently dispersed into the stir zone. Depending on size and location, the dispersive distribution of Al_2O_3 may affect the fatigue life of the FSW joint. It can be seen from the fractographic observation that some of the fractures are initiated from these subsurface inclusions, but only few occur at interior inclusions. Specifically, the inclusions closer to the surface with a larger size are likely to become crack sources and result in inferior fatigue properties. It is observed in this study that the inclusions introduced by FSW process are mainly distributed at the interior of the butt surface (as marked in Fig. 10a). As discussed previously, the effect of the internal inclusions of the welded joints is expected to be negligible.

4.4.2. Incomplete penetration

Incomplete penetration defects might not be detected with normal nondestructive testing (NDT) methods. The incomplete penetration interface is the original butt surface of the plate that remains to be jointed. Inaccessibility of the tool pin to the bottom of welds causes a deficient heat input, leading to incomplete dynamic recrystallization. Incomplete penetration defects always take the form of a root flaw (Fig. 4b). Root flaw should be assumed to be crack-like from the outset of any fatigue loading [10,19]. A high stress concentration appears at the vertex of planar defects, which leads to a significant decrease in the fatigue life. The relationship between the crack-like flaws of different lengths and the tensile strengths of the 2219-T6 aluminum alloy FSW butt joints was investigated in [30], revealing that longer or deeper root flaws favored crack initiation and accelerate the crack propagation rate. Dickerson and Przydatek [19] showed that root flaws up to a certain length can affect the failure performance of the FSW joints significantly. Besel et al. [23] reported that incomplete welding acted as a potential fatigue crack origin and brought about a lower fatigue life.

Table 3 summarizes the fatigue strength of the base metal and the welded joint specimens for 10^7, 10^8, and 10^9 cycles. It is found that there is little difference in the fatigue strengths between the welded joint and the base metal specimens if the welding defects are properly controlled. Moreover, the fatigue properties of the FSW specimen are superior to those of the MIG specimen as reported by [8]. Therefore, the control of the quality of the FSW (especially for incomplete penetration defects) combined with the appropriate NDT are vital to prolong the service life of the FSW structures.

5. Summary

In the study, the VHCF properties of a 7050-T7451 aluminum alloy and its butt welds under ultrasonic fatigue tests are investigated in terms of the microstructural heterogeneity and defects, and the following conclusions can be drawn:

(1) For both the base metal and the FSW joint specimens, fatigue failure still occurs beyond 10^7 cycles and even at 10^9 cycles. The fatigue endurance stress continuously decreases as the number of cycles to failure increases, and no traditional fatigue limit could be determined;
(2) The fracture positions of the base metal specimens are randomly distributed in the parallel part, whereas fatigue failure mainly occurs in the TMAZ and HAZ on the advancing side of the FSW joints. This phenomenon is attributed to the microstructural heterogeneity of the FSW joint. Based on the EBSD analysis and hardness distribution, it is assumed that there exist the weakest link on the advancing side of the FSW joint which leads to inferior crack initiation threshold in the gigacycle fatigue;
(3) Through the fractographic analyses, it is considered that there is a competitive mechanism between the size and location of the inclusions for the VHCF crack initiation in the FSW joints: both the decrease in the distance between the inclusion and the surface and the increase in the inclusion size result in the crack initiation dominated by surface or sub-surface defect, and vice versa. It is observed experimentally that incomplete penetration in FSW joint is equivalent to the crack-like defect, and crack initiation phase of the fatigue life can be negligible.

Acknowledgement

The research is financially supported by the National Science Foundation of China (Grant No. 51375331).

References

[1] Thomas WM, Nicholas ED, Needham JC, Murch MG, Templesmith P, Dawes CJ. G.B patent application no. 9125978.8; December 1991.
[2] Mishra RS, Ma ZY. Friction stir welding and processing. Mater Sci Eng R 2005;50:1–78.
[3] Ericsson M, Sandström R. Influence of welding speed on the fatigue of friction stir welds, and comparison with MIG and TIG. Int J Fatigue 2003;25:1379–87.
[4] Heinz A, Haszler A, Keidel C, Moldenhauer S, Benedictus R, Miller WS. Recent development in aluminum alloys for aerospace applications. Mater Sci Eng A Struct 2000;280:102–7.
[5] Liu HJ, Chen YC, Feng JC. Effect of zigzag line on the mechanical properties of friction stir welded joints of an Al–Cu alloy. Scripta Mater 2006;55:231–4.
[6] Rafi HK, Janaki Ram GD, Phanikumar G, Rao KP. Microstructure and tensile properties of friction welded aluminum alloy AA7075-T6. Mater Des 2010;31:2375–80.
[7] Zhang F, Su XK, Chen ZY, Nie ZR. Effect of welding parameters on microstructure and mechanical properties of friction stir welded joints of a super high strength Al–Zn–Mg–Cu aluminum alloy. Mater Des 2015;67:483–91.
[8] Moreira PMGP, de Figueiredo MAV, de Castro PMST. Fatigue behaviour of FSW and MIG weldments for two aluminium alloys. Theor Appl Fract Mech 2007;48:169–77.
[9] Lomolino S, Tovo R, dos Santos J. On the fatigue behaviour and design curves of friction stir butt-welded Al alloys. Int J Fatigue 2005;27:305–16.
[10] Hobbacher A. Fatigue design of welded joints and components. Cambridge: International Institute of Welding (IIW)/Abington Publishing; 2002.
[11] Wang QY, Lib T, Zenga XG. Gigacycle fatigue behavior of high strength aluminum alloys. Procedia Eng 2010;2:65–70.
[12] Bach J, Höppel HW, Prell M, Göken M. Crack initiation mechanism in AA6082 fatigued in the VHCF-regime. Int J Fatigue 2014;60:23–7.
[13] Meischel M, Stanzl-Tschegg SE, Arcari A, Iyyer N, Apetre N, Phan N. Constant and variable-amplitude loading of aluminum alloy 7075 in the VHCF regime. Procedia Eng 2015;101:501–8.
[14] Liu XL, Sun CQ, Hong YS. Effects of stress ratio on high-cycle and very-high-cycle fatigue behavior of a Ti–6Al–4V alloy. Mater Sci Eng A 2015;622:228–35.
[15] Dai QL, Liang ZF, Chen GQ, Meng LC, Shi QY. Explore the mechanism of high fatigue crack propagation rate in fine microstructure of friction stir welded aluminum alloy. Mater Sci Eng A 2013;580:184–90.

[16] D'Urso G, Giardini C, Lorenzi S, Pastore T. Fatigue crack growth in the welding nugget of FSW joints of a 6060 aluminum alloy. J Mater Process Technol 2014;214:2075–84.
[17] Sutton MA, Yang B, Reynolds AP, Taylor R. Microstructural studies of friction stir welds in 2024-T3 aluminum. Mater Sci Eng A 2002;323:160–6.
[18] Di SS, Yang XQ, Luan GH, Jian B. Comparative study on fatigue properties between AA2024-T4 friction stir welds and base materials. Mater Sci Eng A 2006;435–436:389–95.
[19] Dickerson TL, Przydatek J. Fatigue of friction stir welds in aluminum alloys that contain root flaws. Int J Fatigue 2003;25:1399–409.
[20] Zhou CZ, Yang XQ, Luan GH. Effect of root flaws on the fatigue property of friction stir welds in 2024-T3 aluminum alloys. Mater Sci Eng A 2006;418:155–60.
[21] Matikas TE. Specimen design for fatigue testing at very high frequencies. J Sound Vib 2001;247:673–81.
[22] Wang YL, Pan QL, Wei LL, Li B, Wang Y. Effect of retrogression and reaging treatment on the microstructure and fatigue crack growth behavior of 7050 aluminum alloy thick plate. Mater Des 2014;55:857–63.
[23] Besel M, Besel Y, Mercado UA, Kakiuchi T, Uematsu Y. Fatigue behavior of friction stir welded Al–Mg–Sc alloy. Int J Fatigue 2015;77:1–11.
[24] Jian HG, Yin ZM, Jiang F, Li X. EBSD analysis of fatigue crack growth of 2124 aluminum alloy for aviation. Rare Met Mater Eng 2014;43:1332–6.
[25] Zhou CZ, Yang XQ, Luan GH. Investigation of the microstructure and fatigue properties of friction stir welded Al–Mg alloy. Mater Chem Phys 2006;98:285–90.
[26] Fu RD, Sun ZQ, Sun RC, Li Y, Liu HJ, Liu L. Improvement of weld temperature distribution and mechanical properties of 7050 aluminum alloy butt joints by submerged friction stir welding. Mater Des 2011;32:4825–31.
[27] Jata KV, Sankaran KK, Ruschau JJ. Friction-stir welding effects on microstructure and fatigue of aluminum alloy 7050-T7451. Metall Mater Trans A Phys 2000;31A:2181–92.
[28] Hong YS, Zhao AG, Qian GA, Zhou CG. Fatigue strength and crack initiation mechanism of very-high-cycle fatigue for low alloy steels. Metall Mater Trans A Phys 2012;43:2753–62.
[29] Qian GA, Hong YS, Zhou CG. Investigation of high cycle and very-high-cycle fatigue behaviors for a structural steel with smooth and notched specimens. Eng Fail Anal 2010;17:1517–25.
[30] Li B, Shen YF, Hu WY. The study on defects in aluminum 2219-T6 thick butt friction stir welds with the application of multiple non-destructive testing methods. Mater Des 2011;32:2073–84.